

The Geoid Slope Validation Survey 2014 and GRAV-D airborne gravity enhanced geoid comparison results in Iowa

Wang YM¹, C Becker¹, G Mader¹, D. Martin¹, X Li², T Jiang³, S Breidenbach¹, C Geoghegan¹, D Winester¹, S Guillaume⁴ and B Bürki⁴

¹National Geodetic Survey, Silver Spring, MD USA

²DST Inc. Silver Spring, MD USA

³Chinese Academy of Surveying and Mapping, Beijing, China

⁴Institute of Geodesy and Photogrammetry, ETH Zurich, Switzerland

Abstract

Three Geoid Slope Validation Survey (GSVS) were planned by the National Geodetic Survey (NGS) for validating geoid improvement gained by incorporating airborne gravity data collected by the “Gravity for the Redefinition of the American Vertical Datum” (GRAV-D) project in a flat, a medium and a rough topography area. The flat area one was conducted in Texas and it confirmed that the 1-cm differential accuracy over baseline lengths between 0.4-320 km is achievable by combing the GRAV-D data (Smith et al. 2013). The second survey, GSVS14, was carried out in Iowa in 2014 where the topography is moderate but the gravity has strong variation. Two sets of geoidal heights were computed from GPS/leveling data and observed astrogeodetic deflections of the vertical (DoV) at 204 GSVS14 official marks. They agree with each other in ± 1.2 cm which attests high quality of the GSVS14 data. Three geoid models were computed by combing the satellite gravity model GOCO03/5S with terrestrial and GRAV-D gravity. One additional model, called xGEOID15A had no airborne gravity data, and served as the benchmark to quantify the contribution of GRAV-D to the geoid improvement. The comparisons showed that each model agrees with the GPS/leveling geoid height by 1.5 cm in mark-by-mark comparisons. In differential comparisons, all geoid models have a predicated accuracy of 1-2 cm at baseline length between 1.6 km to 247 km. The contribution of GRAV-D is not apparent due to a 9-cm slope in the western 50 km section of the traverse for all gravimetric geoid models, and it was determined that the slopes have been caused by a 5 mGal bias in the terrestrial gravity data. If that western 50 km section of the testing line is excluded in the comparisons, then improvement by GRAV-D becomes evident: In that case, 1-cm differential accuracy on baselines of any length is achieved by the GRAV-D

enhanced geoid models, a clear improvement over the geoid models without GRAV-D data. GSVS14 confirmed that the geoid differential accuracies are in 1-2 cm range at various baseline length. The accuracy is improved to 1 cm with GRAV-D gravity when the west 50 km line is not included.

With the high accuracy and the traverses over 300 hundred kilometers, the GSVS data are not only useful for validating the local and regional geoid accuracy, but also useful for other high accuracy applications, e.g., GPS height accuracy estimation, development and validation of ultra-precise clocks used in the chronometric leveling.

Key words: Airborne and terrestrial gravity, geoid determination and accuracy, deflections of the vertical, GPS/leveling, astrogeodetic camera, satellite gravity model.

1. Introduction

GSVS14 is a traverse of 200 miles (325km) in the east-west direction, crossing the Midcontinent Rift where the gravity anomaly changes from -60 to 80 mGals. The topography variation is moderate: The elevation decreases from 400 m in Denison in the west to about 200 m in Cedar Rapids on the east side. The traverse contains 204 official marks spaced at about 1 mile (1.6 km). GSVS14 collected long session GPS data (12 - 24 hours) at the official marks and all data were processed and adjusted using the Online Positioning User Service (OPUS) project. At the same time (Summer of 2014), the first order class II spirit leveling (double-run) was conducted between all marks. Absolute gravity was measured at every 10th mark and relative gravity relative gravity was surveyed at the marks between. The Compact Digital Astronomical Camera (CODIAC) of the Swiss Federal Institute of Technology in Zurich CODIAC was hauled and operated off a trailer (Appendix B, Fig. 12). Because of this, many of the official marks will not be accessible to the camera. As such, the camera surveyed at so called “eccentric mark” on the shoulder of the road inside 40 m from the official mark. Astro-geodetic deflections of the vertical (DoV) were computed based on star images taken by CODIAC.

A brief description of data collection and its accuracy estimation is given in section 2. Section 3 is devoted to the computations of the two geoid control profiles from the GSVS14 data. Section 4 describes the computation of four gravimetric geoid models. All geoid models are first compared mark by mark, and then compared differentially with various mark spacing ranging from 1.6 km to 320 km. The results and further comparisons in terms of gravity and DoV are presented in section 5. Discussions and conclusions are given in section 6.

2. Data collected by GSVS14

2.1 Ellipsoidal heights determined from GPS data

The precise geodetic coordinates (latitude, longitude and the ellipsoidal height) at the 204 official marks along the traverse were computed from long session GPS data. In order to have a better GPS control for this project, three temporary CORS (Continuously Operating Reference Stations) were set at the beginning, middle and end of the traverse. A long-session static GPS campaign consisted of two groups of ten receivers with identical antennas. One crew started from west, another from the east of the traverse. Each group occupied 10 neighboring marks simultaneously for two occupation sessions, with each session lasting between 12 and 20 hours. Each static, multi-station session was processed using OPUS Projects. The software used double difference carrier phase observations of GPS data in the ionospheric-free linear combination: it only used L1 and L2 GPS carrier phase data. Tropospheric zenith delays were estimated in piecewise linear fashion with a 2-hour interval. The root mean square errors in the horizontal and vertical coordinates were estimated to be ± 2 cm. Then all session solutions were combined in a least-squares network adjustment, also within OPUS Projects (Wang et al. 2016). After the network adjustment, the formal accuracy estimates for absolute ellipsoid heights ranged from 1 to 2 mm. When these were combined to estimate accuracy of differential ellipsoid heights and clustered into bins of similar distances, it was found that they ranged from 1.4 mm to 2.8mm, with no dependence upon the distance between points. The formal differential error was smaller than 4.4 mm of GSVS11 (Smith et al. 2013).

2.2 Orthometric heights by spirit leveling

Field height differences between the 204 marks were measured by leveling following first order, class II guidelines of the Federal Geodetic Control Committee (Bossler 1984). Absolute gravity was observed at every 10th mark using an A10 absolute gravity meter. Between the marks, a relative gravimeter occupied each mark with 7 repeat observations to reduce random errors. Then the gravity data were adjusted and used to compute the geopotential numbers in a minimally constrained adjustment. The adjustment was fixed to the mark PID4549 with a published height of 289.247 m in the North American Vertical Datum 1988 (NAVD 88) at Ames.

A formal error was assigned to the orthometric height at each mark using the empirical formula $\pm 0.7\sqrt{k}$ mm (Zilkoski et al. 1988), where k is the distance between two marks in km. The maximum error would be 12.5 mm for two marks spaced by 320 km.

2.3 DoV observed by CODIAC

CODIAC is equipped with a GPS receiver which gives low accuracy coordinates. A more precise location of the camera (to about 0.3 m) is needed to determine precise DoVs. This requirement was fulfilled by utilizing the Iowa Real Time Network (IaRTN). Two one-minute RTN observations were collected at each eccentric mark at the beginning and end of the DoV observation sessions. To check the accuracy of the RTN coordinates which are used to determine the geolocation of CODIAC, 47 of the 204 official marks were also observed by one-minute RTN observations, and compared to the 12 to 24 hour GPS long session data. The differences in geodetic coordinates of the two methods are in the range of 2-3 cm in the horizontal and vertical directions (Wang et al. 2016), which correspond to an error of 0.001" in the geodetic latitude and longitude. Note that one mark (GSVS 167), which shows an ellipsoidal height difference of about 30 cm, is considered to be an outlier and was removed from the coordinate comparison.

The CODIAC camera is an updated version of the DIADEM camera used in GSVS11 (Bürki 2015, personal communication). Automated leveling of the camera was added to make it more user-friendly, without to change the main structure of the camera. Therefore, the errors listed in Table 1 and 2 in Smith et al.

(2013) should still apply. However, this is a new camera system and it was used in a different area, thus it is worthwhile to have this error estimate checked.

The CODIAC camera collected star images at 204 eccentric marks. The camera is equipped with two pairs of tilt meters of types Lipmann and Wyler. Each pair of tilt meters is used in a solution to determine astronomical latitude and longitude. These two solutions provide a measure of precision and consistency of the instrument. The following are the statistics of the solution differences.

Table 1. Statistics of differences of north-south (ξ) and east-west (η) components of DoV obtained from the solutions using different couples of tiltmeters – the statistics are calculated as results of 480 solutions and units are in arc-second.

	ξ	η
<i>Mean</i>	0.000	0.000
<i>RMS</i>	0.013	0.015
<i>Min</i>	-0.050	-0.090
<i>Max</i>	0.050	0.090
<i>(*)</i>	0	2

()*: numbers of solutions having differences larger than 0.05 arc-second

Table 1 shows a very good agreement between the solutions using different couples of tiltmeters. The RMS values of differences are around one hundredth of an arc-second. This is one order smaller than the formal accuracy of the camera (0.1"). Extreme differences do not exceed 0.05" along the north-south direction, but there are two solutions having differences larger than 0.05" along the east-west direction.

To test the repeatability and environmental effects on the system, such as changes in the atmospheric conditions, every 20th mark was re-observed after all marks were observed. A total of 11 marks, together with three marks with some

uncertainty concerns, were reoccupied. The statistics of the differences are shown in Table 2.

Table 2. Statistics of differences of north-south and east-west components of DoV determined using the repeated observations at 14 marks, with 4 solutions at each reoccupied mark. Units are in arc-seconds.

	ξ	η
<i># of solutions</i>	56	56
<i>Mean</i>	0.000	0.000
<i>RMS</i>	0.040	0.049
<i>Min.</i>	-0.070	-0.089
<i>Max.</i>	0.061	0.085
<i>(*)</i>	15	23

In comparison with Table 1, the RMS values are nearly tripled. Notice that the reoccupation happened after the completion of the DoV survey which took nearly 40 calendar days. The increased differences could be caused by changes in atmospheric conditions as well as all of the error sources listed in Table 5 of Smith et al (2013). Still, the RMS values of the solution differences are smaller than 0.05" for both components at the re-observed marks. Based on these statistics, one may conclude that DoV obtained by the CODIAC camera in Iowa should have an accuracy of $\pm 0.05''$ for its north-south and east-west components, about the same as DIADEM used in GSVS11.

3. Control geoid profiles computed from GPS/leveling and DoV data

3.1 GPS/Leveling geoid profile

The ellipsoidal and orthometric heights at the GSVS14 official marks were computed from the GPS and spirit leveling data as described in section 2. Using these heights, the geoid undulation at mark i , N_i^G , can be computed as

$$N_i^G = h_i - H_i \quad (1)$$

where h_i is the ellipsoidal height determined by GPS and H_i is the **Helmert** orthometric height determined by leveling. This geoid height, computed at the 204 marks, is hereafter called the “GPSL geoid profile”. Noticing that the leveling adjustment is tied to the bench mark PID4549 in NAVD 88, the geoid undulation computed by (1) is biased when it is compared with gravimetric geoid models. Because the bias is not known accurately, the geoid comparisons can only be made in relative sense for profile comparisons and in differential sense for the slope validation.

It is reasonable to assume that errors in GPS and leveling are uncorrelated, the *differential accuracy* of the GPSL geoid profile σ_k^G at a given spacing k can be computed as

$$(\sigma_k^G)^2 = (\sigma_k^h)^2 + (0.7\sqrt{k})^2 \quad (2)$$

where σ_k^h is the error variance of differential ellipsoidal height.

3.2 Geoid profile by integrating the DoVs

Fig. 1 shows the north-south (Xi) and east-west (Eta) components of the DoV, and the height variation along the test line.

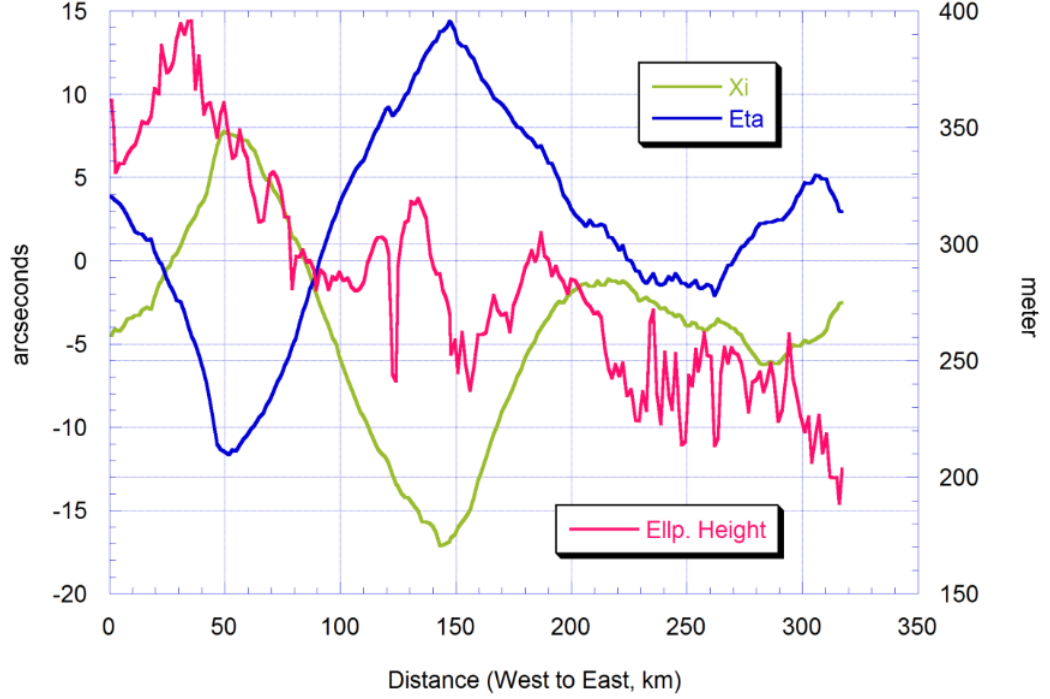


Fig. 1 The north-south (Xi) and east-west component (Eta) of DoV along the GSVS14 traverse. Since the traverse is directed east-west, the component Eta contributes the most to the geoid heights. The elevation decreases gradually from 400 m in Denison to 200 m in Cedar Rapids.

By inspecting the topographic variation and the DoV profile, one can see that the two are not correlated in the long wavelength. The change of Eta from -12" to 15" is caused mostly by the Midcontinent Rift, a high density mass structure deep in the crust, with little topographic signature.

The DoV values shown in Fig. 1 are the angular differences between the plumb line and the normal to the ellipsoid at the eccentric marks on the Earth surface. These values could be reduced to the geoid by correcting the curvature of the plumb-line, and then geoid differences could be computed by integrating the DoV values on the geoid (Heiskanen and Moritz 1967, p. 197). However, the height anomaly can be computed using the surface DoV values directly. Instead of the plumb-line correction, the direction of the normal gravity vector is computed at the observation point on the Earth surface. The angle between the normal plumb-line and the gravity vector at the observation point is called the dynamic DoV (Hofmann-Wellenhof and Moritz 2006, p. 336) and is defined by:

$$\xi^d = \xi - 0.17'' h \sin 2\phi, \quad \eta^d = \eta \quad (3)$$

where ξ^d and η^d are the components of dynamic DoV along a north-south and the east-west directions, respectively; h is the ellipsoidal height in km.

Using related equations in (ibid. p. 338), the height anomaly difference between two marks can be computed by integrating the dynamic DoV and the gravity anomaly along the traverse. Notice that the DoVs are sampled at a distance of 1.6 km in GSVS14, thus the line integrals have to be approximated by summations, which introduces an omission error. To reduce the accumulated omission error along the line, a reference gravity model EGM2008 (Pavlis et al. 2012) is used. At a given point i , the reference DoVs, still at the Earth's surface, ξ_i^{Ref} and η_i^{Ref} are computed from the reference model, and then removed from the observed dynamic DoV by:

$$\delta\xi_i = \xi_i^d - \xi_i^{\text{Ref}}, \quad \delta\eta_i = \eta_i^d - \eta_i^{\text{Ref}} \quad (4)$$

Resulting in $\delta\xi_i$ and $\delta\eta_i$, the residual dynamic DoV components at the mark i .

The geoid height N at a given point K from the starting point ($K = 0$) can be computed from the residual dynamic DoV components, by:

$$N_K = \delta\zeta_K + \zeta_{\text{Ref}} + \delta_K \quad (5)$$

where ζ_{Ref} is the height anomaly computed from the reference model, δ_K is the geoid-quasigeoid separation term (Hoffmann-Wellenhof and Moritz 2006, eq. (8-116)), $\delta\zeta_K$ is the residual height anomaly computed by (cf. *ibid.* p. 337):

$$\delta\zeta_K = \sum_{i=0}^K \delta\chi_i + \sum_{i=0}^K \delta v_i \quad (6)$$

where

$$\delta\chi_i = -\int_i^{i+1} \delta\varepsilon ds \approx -\frac{\delta\varepsilon_i + \delta\varepsilon_{i+1}}{2}(s_{i+1} - s_i), \quad (7)$$

and where s_i is the distance between the point i and the starting point, $\delta\varepsilon_i$ is the projection of DoV along the line segment between point i and $i+1$, given by:

$$\delta\varepsilon_i = \delta\xi_i \cos \alpha + \delta\eta_i \sin \alpha, \quad (8)$$

where α is the azimuth that can be computed by Eq. (2-388) in *ibid.* p. 119.

The quantity δv_i of equation (6) is given by:

$$\delta v_i = -\int_i^{i+1} \frac{\delta\Delta g}{\gamma} dh \approx -\frac{\delta\Delta g_i + \delta\Delta g_{i+1}}{2}(h_{i+1} - h_i), \quad (9)$$

where

$$\delta\Delta g = \Delta g - \Delta g_{Ref}. \quad (10)$$

and Δg_{Ref} is a reference anomaly synthesized from the reference model. For a moderate topography, the 2nd term in (6) is very small. For instance, it only reaches a maximum of 3 mm for GSVS14.

Using the observed DoV data, gravity observed along the line and EGM2008 as a reference field, geoid heights at the eccentric marks are computed using equations (3) – (10). Since the residual height anomaly at the first mark is zero, the DoV geoid profile has the same geoid height as the reference field at this mark. Notice there is a bias between the EGM2008 geoid height and the one of GPSL. For relative geoid comparison, this bias subtracts out. Fig. 2 illustrates the GPSL and DoV geoid height profiles and their differences after removing the bias.

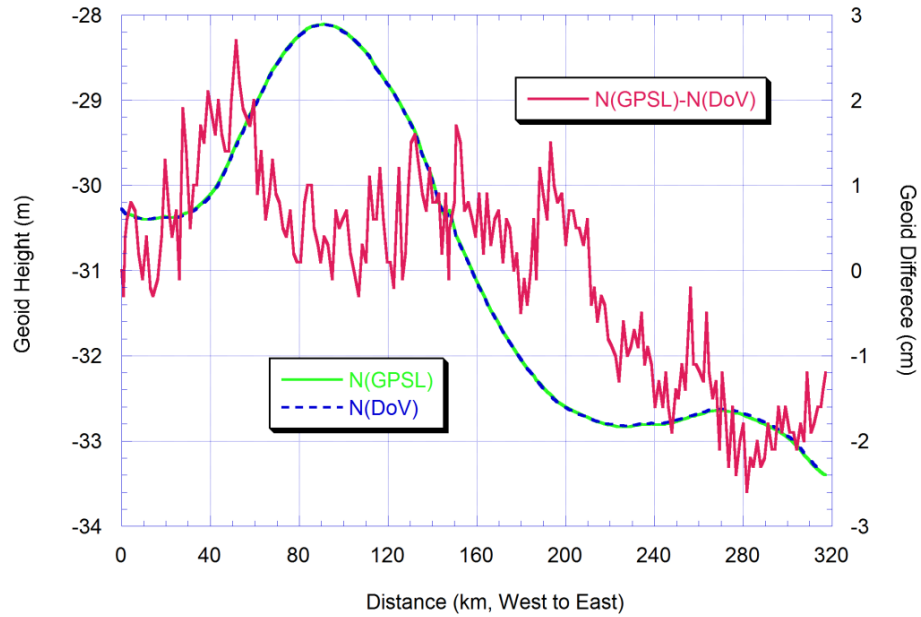


Fig. 2 GPSL vs. DoV geoid profiles and their differences (Red curve)

The DoV geoid profile agrees very well with the GPSL profile. The standard deviation (STD) of the differences at the 204 marks is merely ± 1.2 cm, which is at the same level as the formal accuracy of GPSL. This verifies the high accuracy of both GPSL and DoV control data sets. However, by inspecting the geoid differences in Fig. 2, a slope of $3.6 \text{ cm} / 317 \text{ km} = 0.11 \text{ ppm}$ in the geoid height differences is seen, which is most likely caused by the systematic errors in the DoV data, for reasons explained below. This tilt is about one third of that seen in the GSVS11 line, where the tilt exceeded 10 cm (Smith et al. 2013; Wang et al. 2013). The smaller systematic error in the GSVS14 DoV data may be due to improvement in CODIAC, such as the use of the auto-level mechanism and two new tilt-meters, the precise calibration of the system (Appendix B), and modified survey procedure. In addition, better environmental conditions in GSVS14, such as the almost East-West direction of the GSVS14 traverse and favorable atmospheric conditions (less humidity and temperature variation than in Texas where GSVS11 was conducted) may have played a role in reducing the systematic errors of the DoV data.

Assuming that the GPSL geoid profile is tilt-free, the tilt in the DoV geoid profile accounts for a bias in the DoVs of $0.11 \text{ mm} / \text{km} = 0.023''$. This is on the order of the systematic error sources listed in Tables 5 of Smith et al. (2013), e.g., the celestial calibration error. Thus we conclude that the random and systematic

errors of CODIAC are estimated as $\pm 0.05''$ and $\pm 0.023''$ for the north-south and east-west components of DoV, respectively.

4. Gravimetric geoid models used in the validation

The terrestrial gravity in the test area has a fairly good coverage with varying data distribution density. The GRAV-D flight has an average altitude of 6.3 km and the data were collected at the same time period as GSVS14. The distribution of gravity data and the location of the GSVS14 traverse are shown in Fig. 3.

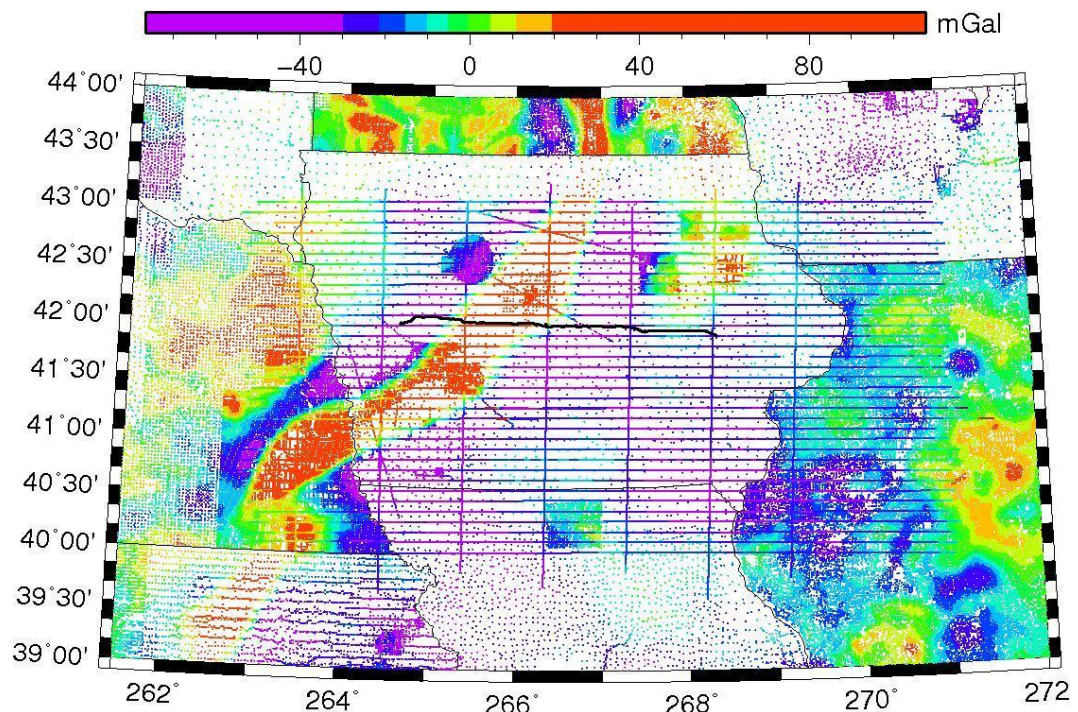


Fig. 3 Gravity anomalies in the test area. Each dot represents one surface gravity measurement and lines in the east-west and north south directions represent airborne data. The 4 slanted lines crossing the Midcontinent Rift are surface gravity measurements. The east-west black line is the GSVS14 traverse.

Using the data in Fig. 3 and the latest satellite gravity models GOCO3S and GOCO5S (Mayer-Gürr et al. 2012, 2015), four different geoid models were computed (as seen in Table 3). The first, xEGM15, is computed using the EGM2008 approach to the same resolution and format. The xEGM15 model incorporates the GOCO03S satellite gravity model, NGS terrestrial gravimetry, and GRAV-D airborne data. The construction of this model is very similar to that of the xEGM-GA model as described in Smith et al. (2013). Essentially, xEGM15

results from the spectral combination of three separate global geopotential models, two of which are ‘disposable/temporary’ and are only created to support the final combination. The first temporary model is identical to EGM2008, except in the survey area where the model has been updated to reproduce the NGS terrestrial data that surrounds the GSVS14 line. The second temporary model is very similar, in that it is also identical to EGM2008, except in the GRAV-D survey area where the model has been updated to reproduce the GRAV-D airborne data that was collected over the GSVS14 line. The third model is the GOCO03S satellite gravity model. All three models are combined at the coefficient level, using ‘error degree variance’ models that have been customized for each data set in the GSVS14 local area (Jiang and Wang 2016). Fig. 4 shows the spectral weights used for the combination.

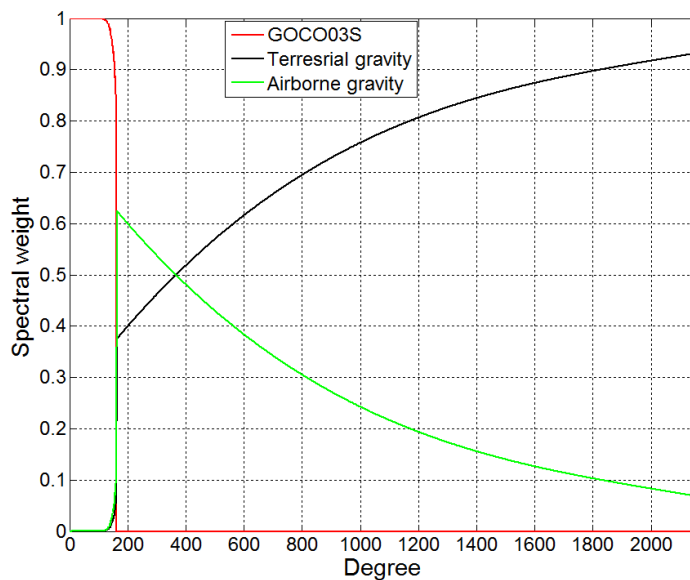


Fig. 4 Spectral weights used for geoid model xEGM15

As compared to the spectral weights used by xEGM-GA (Smith et al. 2013, Fig. 9), the contribution of airborne gravity is not limited to a narrow frequency band between harmonic degree 180 to 420, but from degree 160 to 2160 because of a much lower flight altitude (6.3km) of GRAV-D in comparison to the 11 km flight altitude over GSVS11.

The second geoid model, xG15, is computed by taking the xEGM15 geoid model, and augmenting this with high-resolution (1’x1’) gravimetry and forward-modelling of a Residual Terrain Model or ‘RTM’ (Forsberg 1984). In this

way, the xG15 geoid is computed by using xEGM15 as a ‘reference model’ in the classic remove-restore approach.

The next two geoid models, xGEOID15A and xGEOID15B, were not computed specifically for this study. Instead, since 2014, NGS is required to compute two experimental geoid models for the United States and its territories. The most important of these is designated as the ‘B’ model, and incorporates any gravimetric data sets available at the time, including all of the GRAV-D airborne data that is processed and ready for use. The corresponding ‘A’ model is intended to be identical to the ‘B’ model, except that it excludes the GRAV-D airborne data. In this way, the differences between corresponding ‘A’ and ‘B’ models show the extent to which the GRAV-D airborne data is contributing to the current geoid solution.

Similar to xG15, the xGEOID15A and xGEOID15B geoid models are both obtained by a first computing a spherical harmonic reference model, and then augmenting this with high-resolution gravimetry and RTM information. For xGEOID15A, the supporting xGEOID15A reference model is a combination of EGM2008 and the GOCO05S satellite gravity model. This combination is achieved in two steps. The first step involves a highly localized combination in the space domain, in which geographically specific and degree-wise error models are applied over a small spherical cap. The final combination is performed at the coefficient level. More information can be found on the NGS xGEOID15 website (<http://beta.ngs.noaa.gov/GEOID/xGEOID15/>). For xGEOID15B, any additional GRAV-D airborne data is propagated into the final geoid model through its supporting reference model. Thus the reference model for xGEOID15B is similar to that for xGEOID15A, except that EGM2008 has been replaced with a ‘disposable/temporary’ spherical harmonic model that has been augmented with GRAV-D airborne data. Outside of GRAV-D data areas, this temporary model reproduces EGM2008 gravity -anomalies/-disturbances. Within the GRAV-D data areas, the temporary model reproduces a cleaned, adjusted and filtered version of the GRAV-D airborne gravimetry. This temporary model is combined with GOCO05S using the same two-step procedure as was used for xGEOID15A. Once the spherical harmonic reference models for xGEOID15A and xGEOID15B are complete, they are augmented with 1’x1’ NGS gravimetry and RTM

information using the same remove restore methodology as was used for xG15. More information can be found on the NGS xGEOID15 website.

The geoid models used in the validation are summarized in the Table 3.

Table 3 Geoid models used in the validation

Model	Sat. Model	GRAV-D	Resolution	RTM
<i>xEGM15</i>	GOCO3S	Yes	5'	No
<i>xG15</i>	GOCO3S	Yes	1'	Yes
<i>xGEOID15A</i>	GOCO5S	No	1'	Yes
<i>xGEOID15B</i>	GOCO5S	Yes	1'	Yes
<i>EGM2008</i>	ITG-GRACE03	No	5'	No
	S			

5. Geoid Validation

5.1 Geoid profile comparisons

We start with the comparisons of geoid models, mark by mark, along the GSVS14 traverse. The differences (Model – GPSL) are shown in Fig. 6. Since the leveling data were constrained to a mark of NAVD 88, there are about 80 cm biases between the geoid models and the GPSL geoid profiles. In addition, EGM2008 and xEGM15 used the W_0 value of $62,636,855.69 \text{ m}^2\text{s}^{-2}$, while xGEOID15A/B used a new value $62,636,856.0 \text{ m}^2\text{s}^{-2}$. The difference between the two W_0 values results in a bias of 3 cm between those geoid models of GSVS14 in the test area.

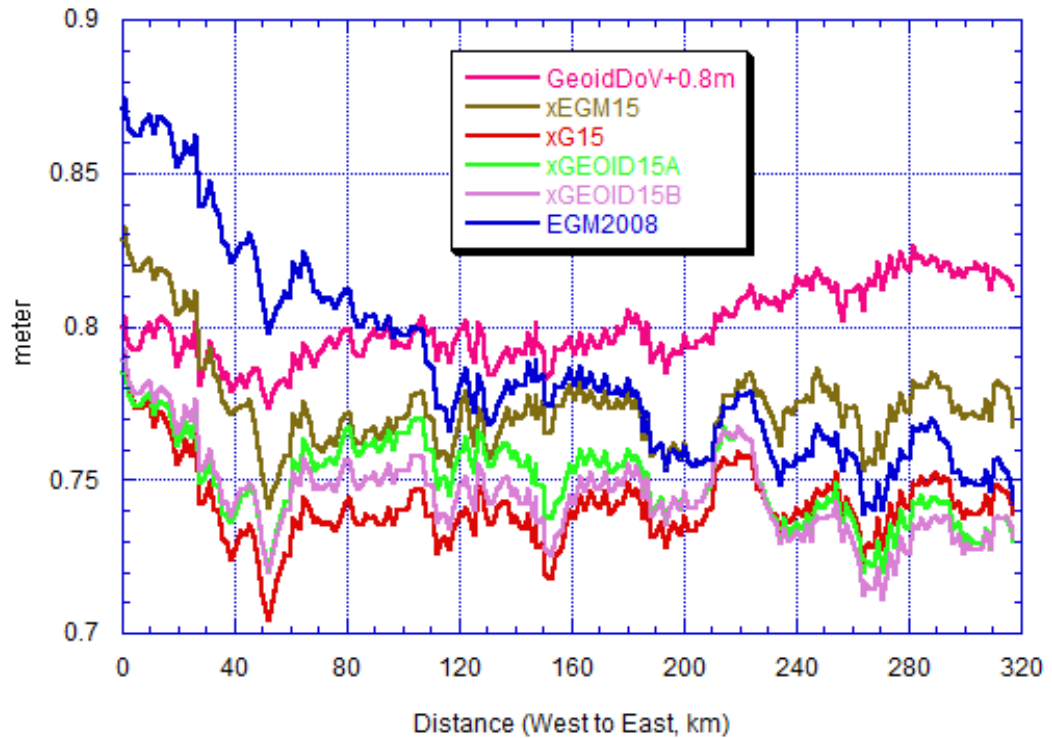


Fig. 5 Geoid differences between the control GPSL profile and various models. The 75 cm biases are caused by the use of different geopotential numbers for geoid modeling and NAVD 88. 80 cm is added to GeoidDoV to make the graph more readable.

By inspecting the graph, one can see that EGM2008 has a large (~12 cm from west to east) tilt along the traverse, a trend similar to that of the topography. This trend is of long wavelength nature which could be caused by errors in satellite model and/or the gravity data reduction in the Rocky Mountains near GSVS14. Another observation is that all gravimetric models have about a -9 cm slope along the western 50 km of the traverse, closest to the Midcontinent Rift, where the gravity anomaly changes from negative to positive (Fig. 3) and the topography reaches its peak. The large slopes have not been corrected by the latest satellite models GOCO03S/5S nor GRAV-D data. It was shown recently (Li et al. 2016) that large errors in terrestrial gravity over Lake Michigan were corrected by combining a satellite gravity model and GRAV-D data. The immediate question is why the same did not happen this time. The difference between Lake Michigan and the western 50 km along GSVS14 traverse is that there is no topography over a flat lake surface, thus the gravity and topographic reductions would be the area to look first. In addition, the weight between different data types may be need

fine-tune. These are just speculations at this time, the exact reasons have not been determined and will be investigated outside of this paper.

Carefully inspecting Fig. 4, one can see that there are 2-5 cm dips and bumps at distances of 110, 150, 220, and 260 km along the line, which happen in models with or without the GRAV-D data, as well as in EGM2008. All gravimetric geoid models use the same terrestrial gravity data. Thus, these dips and bumps most likely indicate errors in the terrestrial gravity data. The absence of such relatively large bumps in the difference of the DoV-derived and GPSL control geoid profiles excludes GPS or leveling as a source of these errors. Furthermore, the lack of the large tilt between the DoV-derived and GPSL profiles in the western 50 km further points to the source of the error being terrestrial gravity data, despite the inability of GOCO and GRAV-D to correct it.

The large slopes in the western 50 km of the line have a large impact on the accuracy assessment of geoid models. The statistics of geoid comparisons (to the GPSL profile) with and without the inclusion of these western 50 km are listed in Table 4.

Table 4 Standard deviation of geoid height differences, relative to the GPSL profile, in cm

<i>Geoid model</i>	<i>EGM08</i>	<i>xEGM15</i>	<i>xG15</i>	<i>xGEOID15</i>	<i>xGEOID15B</i>	<i>GeoidDoV</i>
				<i>A</i>		
<i>Whole line</i>	3.4	1.6	1.3	1.4	1.5	1.2
<i>without the west 50 km</i>	2.0	0.9	0.9	1.2	1.1	1.2

Table 4 shows that all geoid models, except EGM2008 agree with GPSL from 1.4 to 1.6 cm at the 204 marks in terms of standard deviation. The dispersion gets much smaller in the comparisons without the western 50 km. The standard deviation of the geoid height differences is reduced from 1.6 cm and 1.3 cm to 0.9 cm for both xEGM15 and xG15. Similar improvement happens for EGM2008 too: the standard deviation values are reduced from 3.4 cm to 2.0 cm. xGEOID15A

outperforms xGEOID15B slightly (1.4 vs. 1.5 cm) for the whole line, but the later performs slightly better without the west 50 km (1.2 vs. 1.1 cm).

5.2 Differential geoid comparisons

In practice, it is significantly more important to check how well the geoid models compare with the GPSL geoid profile *differentially*, over different baseline lengths. An effective way to do that is by binning geoid height differences over different baseline lengths to get the predicted geoid errors (Smith et al. 2013).

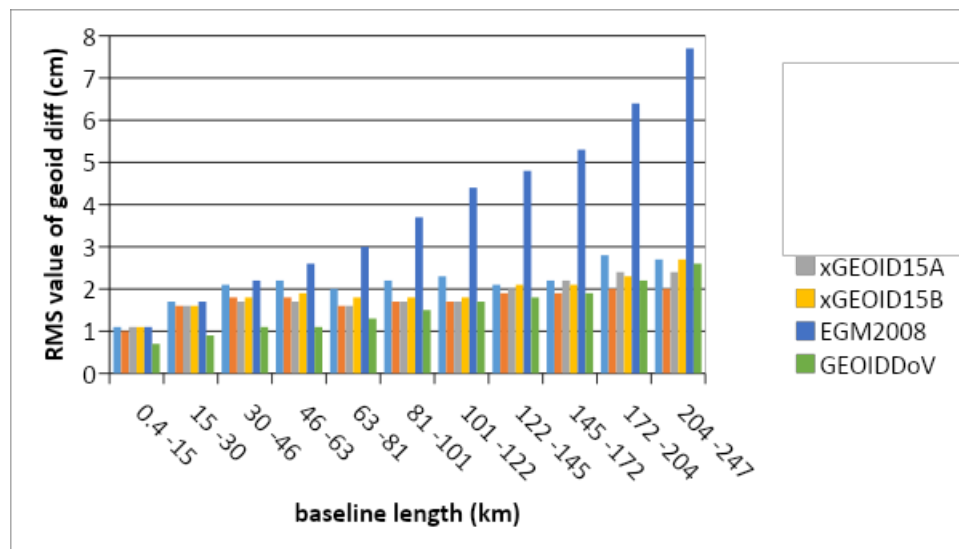


Fig. 6 Variances of geoid differences as a function of baseline length. Number of possible pairs for each bin is around 1800. The last bin (248-340) has significant less number of pairs and it is not shown here.

Fig. 6 shows that the variances of geoid differences are all below 3 cm for all geoid models, except EGM2008. The variances consist of the differential errors in geoid models and GPSL data. Once differential ellipsoid height accuracy and differential leveling accuracy are accounted for, the only remaining error source in the disagreement between the GPSL geoid profile and a gravimetric geoid should be the geoid itself. The estimated geoid errors for selected geoid models are presented in Fig. 7.

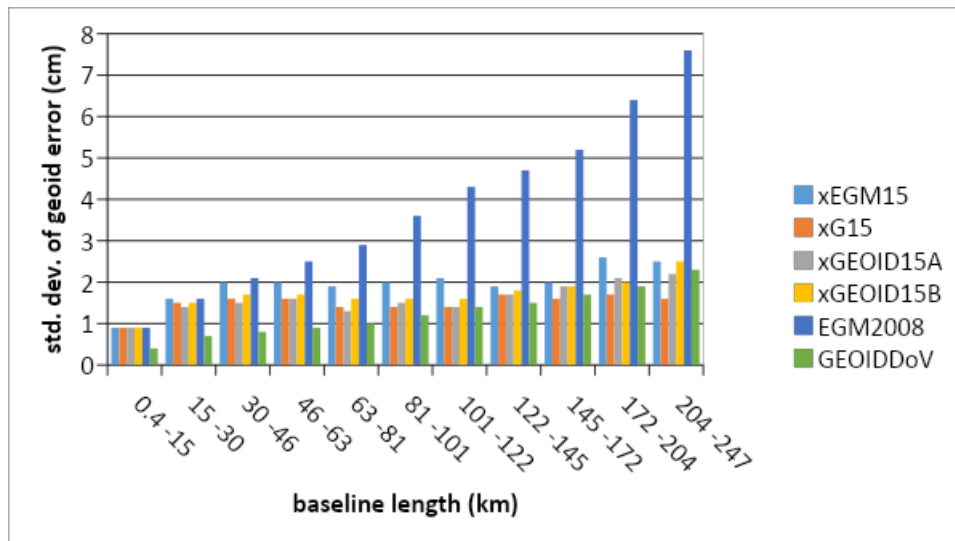


Fig. 7 Predicted differential geoid errors (in cm) as a function of baseline length (in km) for the whole traverse.

Fig. 7 shows that all geoid models have a differential accuracy better than 2.5 cm for baseline of length between 0.4 km to 247 km. Geoid height differences between GPSL and EGM2008 have a 12 cm tilt, thus a similar trend appears in this differential geoid error too. The further the two marks are apart, the larger the differences become and the larger the predicted errors become. The geoid error of EGM2008 increases from 0.8 cm to 7.8 cm with baseline length of 0.4 km and 247 km, respectively. A small slope (0.11 ppm) in the DoV geoid height differences also causes the geoid error to increase nearly linearly from 0.3 cm to about 2.3 cm from the shortest to longest baseline lengths. If the tilt in the DoV geoid profile is removed, the error in the DoV data is purely random, and then the error in the DoV geoid profile would act like a random walk, similar to the behavior of the leveling error. In this case, the error would be 0.2 cm to 0.5 cm for baselines of length 1.6 km to 247 km, which agrees well with the error estimate computed using Eq. (A5).

The second observation is that all high resolution gravimetric geoid models (xG15, xGEOID15A and xGEOID15B) perform at similar accuracies, with only small deviations from one another. All high resolution models have a predicted error ranges from 1 cm to 1.5 cm for baselines shorter than 122 km and slightly increased errors for longer baselines because of the -9 cm slopes in the

western 50 km of the test line. xGEOID15A and xGEOID15B perform nearly the same for all baselines length, but it is troubling to see that the model with GRAV-D (xGEOID15B) does not improve with the model without GRAV-D (xGEOID15A). xG15 uses xEGM15 as the reference model and applied the RTM effect, it performs the best. As we mentioned before that the -9 cm slopes in the western 50 km of the test line have profound impact to the geoid comparisons, thus we redo the statistics without using it.

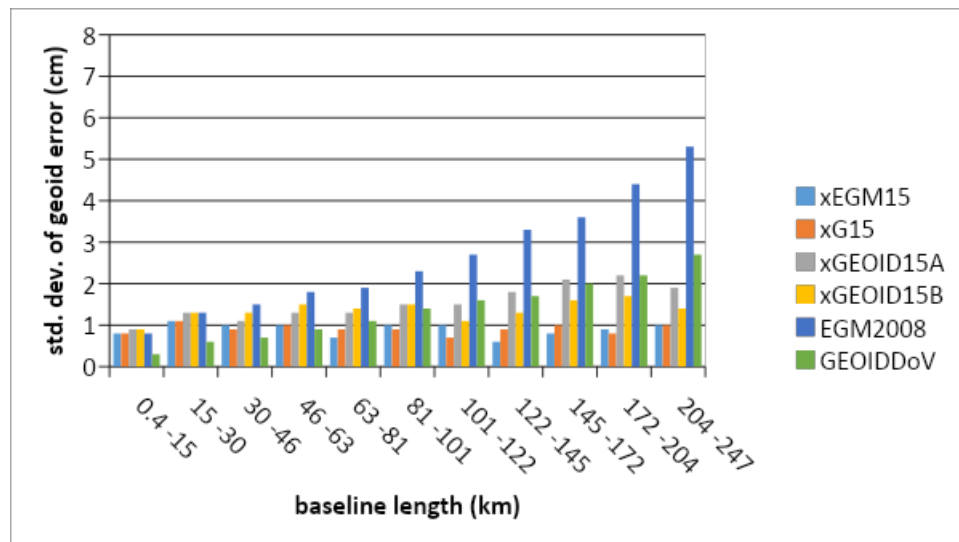


Fig. 8 Predicted differential geoid errors (in cm) as a function of baseline length (in km) without the western 50 km section of the test line.

The geoid accuracy improvement due to the airborne gravity of GRAV-D becomes evident in Fig. 8. The geoid models xEGM15 and xG15 both have an accuracy around 1 cm or better at any baseline length, a 50% to 100% improvement to the whole line comparison. xGEOID15B outperforms xGEOID15A in baselines longer than 101 km, and the former has an accuracy at or better than 1.5 cm for any baseline lengths. Notice that xGEOID15B is 50% worse than xEGM15 or xG15 for baseline longer than 101 km. xEGM15 used GOCO03S and the weights were computed from the error degree variances of each data type (Jiang and Wang 2016); and xGEOID15B used GOCO05S and empirically determined weights (Smith et al. 2013). Disregarding the differences between GOCO03S and GOCO05S in the area, the improvement in xEGM15 may be predominately due to the different spectral weights. Thus, the results demonstrate the importance of the proper weights in the geoid modeling.

In summary, all gravimetric geoid models have an accuracy of 2 cm or better at any baselines. All gravimetric geoid models perform almost the same, with or without the GRAV-D airborne gravity data. The improvement of GRAV-D is not clear because of the -9 cm slopes in the western 50 km section of the traverse where the terrestrial gravity is biased by 5 mGal (see later section for gravity comparison) and is not corrected by GRAV-D for some unknown reasons. If the west section is excluded in the comparisons, the GRAV-D airborne data contribution becomes evident. The long wavelength error in xGEOID15A (Fig. 8 vs. 9) is removed and the predicted accuracy of xGEOID15B outperforms that of xGEOID15A for baselines longer than 101 km. xEGM15 and xG15 perform the best after removing the western 50 km section. Its predicted accuracy is at the 1 cm level or better at any baseline length. Notice that xGEOID15B and xG15 used the same terrestrial and airborne gravity data. The differences between the two geoid models are mainly caused by the different spectral weighting. Spectral weights determined by error degree variances of the satellite model, airborne and terrestrial gravity data seem to give the best result in this case.

5.3 DOV comparison

DoV used in the following comparisons are the angle between the plumb line and the normal to the reference ellipsoid at the eccentric marks on the Earth's surface, called the Helmert DoV. The north-south (ξ) and east-west (η) components of DoV are computed by a spherical harmonic synthesis of EGM08 at the eccentric marks. These components are also computed using the usual spherical formula (Heiskanen and Moritz Eq. 2-204, 1967) at every mark by:

$$\begin{aligned}\xi &= -\frac{1}{\gamma R} \frac{\partial T}{\partial \phi} \\ \eta &= -\frac{1}{\gamma R \cos \phi} \frac{\partial T}{\partial \lambda}\end{aligned}\quad (11)$$

where R is the mean radius of the Earth.

This type of DoV (Jekeli 1999) is of the gravity type and needs to be transformed to Helmert's DoV. Because the magnitude of the corrections is a few thousandths of an arc second, we ignore them in the comparisons. The two

components of DoV of xGEOID15A/B are computed from the slopes of the geoid models and plumb line correction was applied. The following figure shows the differences and the statistics between the observed DoV and the one computed from the geoid models.

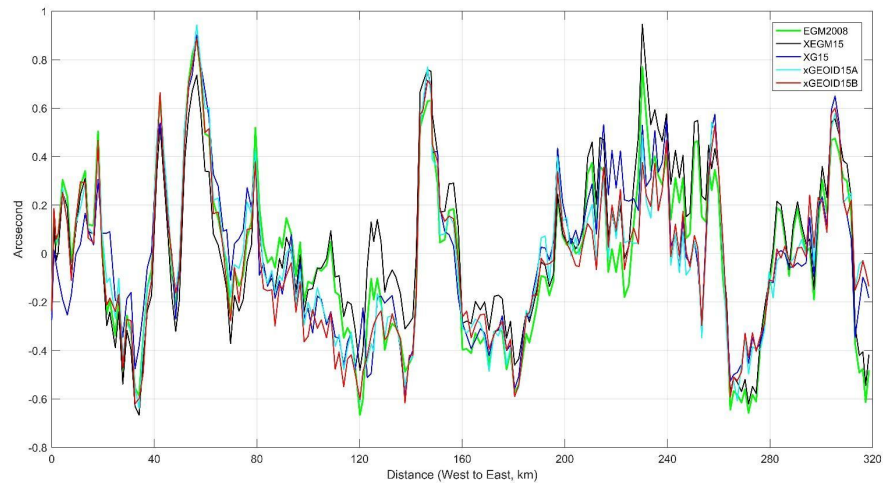


Fig. 9a the N-S component of DoV differences between CODIAC and geoid models.

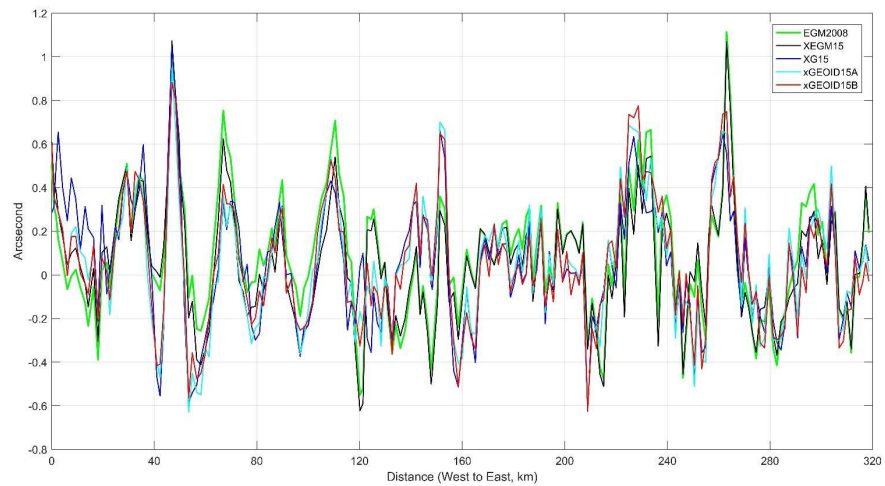


Fig. 9b the E-W component of DoV differences between CODIAC and geoid models.

Figs. 9 a, b show that all models perform similarly, and the large differences happen to be at the same locations. Since the residual DoVs consists

mostly of high frequencies and since GRAV-D airborne data contribution is limited mostly to the medium frequencies, no improvements due to airborne data can be seen in Fig. 9a, b. The statistics of the DoV differences are given in the following table.

Table 5a. Statistics of the DoV differences in the north-south direction, units in arc-seconds.

Model	Mean	RMS	STD	Min.	Max.
<i>EGM2008</i>	-0.02	0.34	0.34	-0.67	0.89
<i>xEGM15</i>	0.03	0.33	0.33	-0.67	0.95
<i>xG15</i>	-0.01	0.32	0.32	-0.59	0.91
<i>xGEOID15</i>	-0.02	0.32	0.32	-0.64	0.94
<i>A</i>					
<i>xGEOID15</i>	-0.04	0.32	0.32	-0.62	0.89
<i>B</i>					

Table 5b. Statistics of the DoV differences in the east-west direction, units in arc-seconds.

Model	Mean	RMS	STD	Min.	Max.
<i>EGM2008</i>	0.09	0.29	0.30	-0.55	1.11
<i>xEGM15</i>	0.06	0.28	0.28	-0.62	1.07
<i>xG15</i>	0.06	0.29	0.29	-0.63	1.04
<i>xGEOID15</i>	0.06	0.29	0.29	-0.63	0.95
<i>A</i>					
<i>xGEOID15</i>	0.06	0.29	0.29	-0.62	0.88
<i>B</i>					

5.4 Gravity comparison

GSVS14 collected gravity data at 204 official marks with an accuracy of ± 0.05 mGal with geolocation accuracy of 1-2 cm horizontally and vertically. This data set is used as a ground truth for the gravity comparison. Gravity anomalies are synthesized using EGM2008 and xEGM15 at the mark locations. The gravity anomalies of xG15 and xGEOID15A/B are computed from its residual grids and

their reference fields, and all gravity anomaly profiles along the test line are presented in Fig. 10.

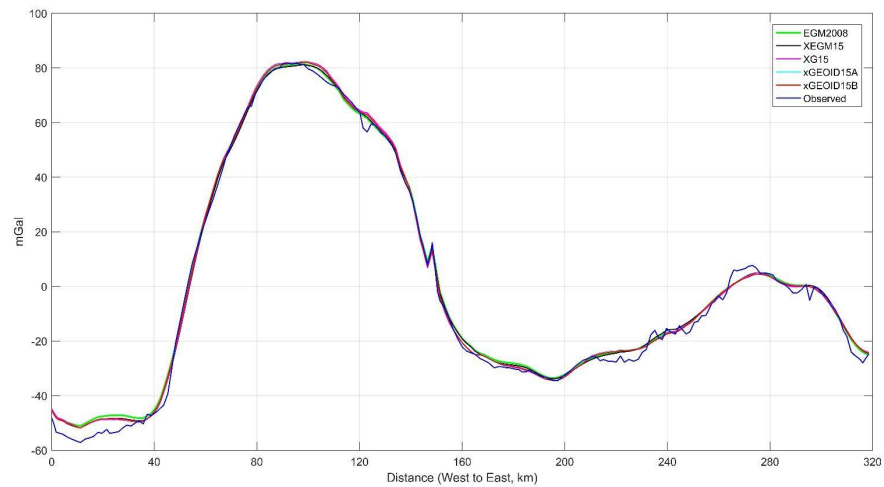


Fig. 10 Surface gravity anomalies along the GSVS14 traverse

The gravity anomaly changes about 140 mGal crossing the Midcontinent Rift – from negative 60 to positive 80 mGal. Gravity anomalies of all geoid models, including EGM2008 match the observed gravity anomaly closely, but are missing some fine details. In comparison with Fig. 5, one can see immediately that the fine details in gravity have one-to-one correspondence with the dips and bumps in the geoid differences. The largest differences between the observed and modeled gravity anomalies happen at the western part of the traverse where the maximum geoid difference occurs.

The residuals between geoid-model-implied gravity anomalies and gravity anomalies based on observed gravity from GSVS14 are shown in Fig. 11. Although there are large fluctuations in that graph, the mean difference is around a mean of 1.1 mGal, with about 2.3 mGals standard deviation. The residual gravity anomalies associated with every geoid model, with or without the GRAV-D data, have a mean of about 5 mGal at the western 30km section of the line. Because the same terrestrial gravity went in to every geoid model, but the residuals in Fig. 12 are with respect to newly observed gravity just for GSVS14, this confirms that the

large discrepancies at the western section of the line are due to this large error in the terrestrial gravity data in the area.

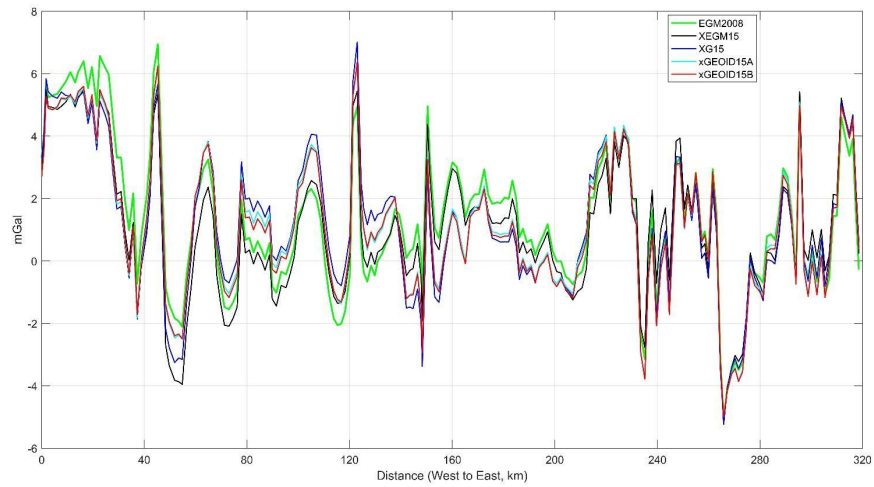


Fig. 11 Gravity differences along the GSVS14 traverse

Table 6. Statistics of gravity differences (Model – Observed). Units in mGals

Model	Mean	RMS	STD	Min.	Max.
<i>EGM2008</i>	1.3	2.7	2.3	-5.1	6.9
<i>xEGM15</i>	1.0	2.5	2.2	-5.2	5.5
<i>xG15</i>	1.1	2.6	2.3	-5.1	7.0
<i>xGEOID15</i>	1.1	2.5	2.3	-5.0	6.3
<i>A</i>					
<i>xGEOID15</i>	1.1	2.5	2.3	-5.0	6.4
<i>B</i>					

Fig. 11 and Table 6 show three things. Firstly, the surface gravity anomalies of all gravity models are accurate to about 2.5 mGal, relative to newly acquired gravity. Secondly, since the existing terrestrial gravity is of good quality and the GRAV-D data contributes mostly in medium wavelengths, little improvement is seen in high frequency variances by adding GRAV-D data. Third, the errors in terrestrial gravity data fluctuate around the mean. They have spatial resolutions ranging from few km to 20 km, and cannot be corrected by satellite

models or GRAV-D. The use of high-resolution DEMs could provide higher frequency signal of the gravity data and reduce these errors (Higgins et al. 1996).

6. Conclusions

The first Geoid Slope Validation Survey in Texas confirmed that 1-cm relative geoid accuracy can be achievable in a flat coastal region over baselines from 0.4 – 320 km (Smith et al. 2013). The second survey was conducted in Iowa where the topography is moderate and the elevations decreased gradually from 400 m in the west to 200 m in the east. The traverse crosses the Midcontinent Rift, which causes gravity anomaly changes of about 140 mGal. Two control geoid profiles were computed from the GSVS14 data, one from GPS and leveling data, and another from DoV using the method of remove-restore, where EGM2008 to degree and order 2160 was used as the reference model. The two geoid profiles agree to within ± 1.2 cm in the geoid undulation, attesting a high accuracy of the collected data sets. However, there is a slope of 0.11 ppm in the geoid differences along the 320 km traverse. If we assume that the GPSL geoid profile is tilt-free then this slope implies 0.023" bias in the DoV data. A bias in the DoV data is not unexpected, as one was seen also in GSVS11. However, this is about one third of the bias of DIADEM used for GSVS11. The improvement is probably due to the auto-leveling mechanism of CODIAC, and the use of two new tilt-meters. The environmental conditions (less humidity and temperature variation, and the direction of the traverse) may have played a role, too. The random and systematic errors of the DoV data are estimated as 0.05" and 0.023" for CODIAC based on the repeated observations and the GPSL geoid profile comparisons. If the systematic error is corrected, the DoV geoid profile should have an accuracy of 0.24 mm per square root of the distance between two marks based on the error propagation law (Eq. A5) which implies a maximum error of 0.5 cm over the GSVS14 traverse.

Three GRAV-D airborne data enhanced geoid models xEGM15, xG15 and xGEOID15B were selected for the GSVS14 validation. For quantifying the GRAV-D contribution, xGEOID15A which is computed in a nearly identical way as xGEOID15B, but without airborne data, is included in the comparisons. EGM2008, which has been used in many ways for geoid computations, is also

included. The comparisons show that EGM2008 has a slope of 12 cm along the traverse and it has the same trend as the topography. All other geoid models perform nearly the same as one another in the comparisons. They agree with the GPSL geoid profile by about 1.5 cm in mark-by-mark comparisons. In differential comparisons, all geoid models have a predicted accuracy of 1-2 cm for baselines of length ranging from 1.6 km to 247 km. In these comparisons, the contribution of GRAV-D is not apparent. The reasons for this may be that the comparisons are distorted by the -9 cm slopes in geoid differences in the western 50 km section of the test line in all geoid models. The gravity comparison confirms that there is about 5 mGal error in the terrestrial gravity that may be the major contributor to the -9 cm slopes. It has been shown that the GRAV-D data corrected a similar type of data bias over Lake Michigan (Li et al. 2016). It is not clear why GRAV-D data has not corrected the error in terrestrial gravity data in the western section of GSVS14 test line. Since there is no topography over Lake Michigan, the topography and gravity reduction could be the prime suspects.

If the western 50 km section is excluded in the comparisons, the improvement due to GRAV-D airborne data becomes evident. The geoid models with and without GRAV-D data, namely xEGM15, xG15 and xGEOID15A, agree with the GPSL geoid profile to 0.9 cm, 0.9 cm and 1.2 cm, respectively in point by point comparisons. The predicted differential geoid accuracy improves even more clearly. xEGM15 and xG15 have a predicted differential accuracy of 1.0 cm or better, which outperforms xGEOID15A overall baseline lengths.

The primary goal of GSVS projects is to validate the differential geoid improvement by using the GRAV-D airborne data. At the same time, the traverse can also be used to identify problem areas in the geoid models. The gravity comparisons show that the errors in terrestrial gravity relate directly to the dips and bumps in the geoid differences. Thus the GSVS data can be used to aid further improvement in geoid modeling.

Recently the chronometric leveling with ultraprecise clocks has been making significant progress and can reach cm-accuracy in near future (Flury 2016). The heights, more specifically the geopotential differences at GSVS marks are accurate to about 1-cm between any pair of marks, and could be used as

testbed for the developing and validating the clocks used in chronometric leveling. The data are also useful for other high accuracy applications, such as validating the accuracy of ellipsoidal height obtained from the OPUS project (e.g., Wang et al. 2013).

Appendix A. Errors of the DoV geoid profile

The errors in DoV consist of systematic and random. They affect the geoid accuracy differently. The systematic error has a much more profound impact on the geoid accuracy because it accumulates with respect to the length of the line linearly. In order to have a ± 10 mm geoid accuracy over a 325 km line, the systematic error in DoV has to be smaller than 0.03 mm/km = $0.0063''$. This is in the range of the systematic errors in star catalog, anomalous refraction and others (Smith et al. 2013, Table 5). The error sources are difficult to locate and correct. An effective way to reduce the systematic error is to use a satellite gravity model combined with a high degree and order spherical harmonic coefficient model. Because the systematic error is (at least) very long wavelength, the satellite gravity models which are accurate in this frequency band can be used to control this type of error. The use of a high degree and order spherical harmonic coefficient model is to reduce the aliasing of high frequencies into lower frequencies of the gravity field.

Assuming the systematic error is removed, the remaining error $\varepsilon(x)$ in DoV is only the random error which has the property

$$E[\varepsilon(x)\varepsilon(x')] = \sigma_0^2 \delta(x, x') \quad (\text{A1})$$

where $E[\cdot]$ is the expectation operator (Moritz 1980, p.76), σ_0^2 is the variance of random error in DoV data, and $\delta(x, x')$ is the delta function.

Ignoring the last term in Eq. (6) and assuming the geoid-quasigeoid separation term in (5) is free of error, the geoid error $\theta(K)$ at the mark K can be expressed as

$$\theta(K) = \int_0^{d(K)} \varepsilon(x) dx \quad (\text{A2})$$

where $d(K)$ is the distance from the starting point to the mark K .

The geoid error variance at mark K is

$$\begin{aligned} \sigma_N^2(K) &= E[\theta(K)\theta'(K)] \\ &= E\left[\int_0^{d(K)} \varepsilon(x) dx \int_0^{d(K)} \varepsilon(x') dx'\right] \\ &= \int_0^{d(K)} dx \int_0^{d(K)} E[\varepsilon(x)\varepsilon(x')] dx' \\ &= \sigma_0^2 d(K) \end{aligned} \quad (\text{A3})$$

The root mean square of geoid error variance is then

$$\sigma_N(K) = \sigma_0 \sqrt{d(K)} \quad (\text{A4})$$

Eq. (A4) shows the geoid error is linearly proportional to the square root of the length of the line. It is in the same form as the empirical error formula for spirit leveling (Zilkoski et al. 1988). For CODIAC, 0.05 arcsecond error in DoV would cause the geoid error by

$$\sigma_N = \pm 0.24 \sqrt{d} \text{ (mm)} \quad (\text{A5})$$

where d is in km. This error is about one third of the leveling of the first order class II which has a formal accuracy ± 12.5 mm over the same length of the traverse. The error increases gradually from few mm to 17.0 mm for a 5000 km line crossing the US continent from west to east, if the systematic error is properly corrected. For the GSVS14 traverse (length of 320 km), the maximum error would be ± 4.3 mm. This agrees quite well with the empirical results in Table 9 (Hirt and

Flury 2008), taking into account the fact that CODIAC is nearly 50% more accurate than the camera used in their study.

Appendix B. The Compact Digital Astrometric Camera CODIAC

The Compact Digital Astrometric Camera CODIAC (Fig. 13) is a new zenith camera system entirely designed, developed and manufactured at the Institute of Geodesy and Photogrammetry of ETH Zurich (Guillaume 2015). The principal objective behind the development of a new system was to replace the system DIADEM with a system of reduced size and costs, based on commercial modern components, that provides the same level of accuracy as DIADEM (Somieski 2008). In addition, it is designed with almost industrial standards in order to facilitate the use by non-astrogeodetic experts, to increase the performance in terms of productivity.



Fig. 12 The CODIAC system.

The two main components of the hardware consist of the astrometric (optical) part and the tilting part. The astrometric part is formed by a Riccardi-Honders Astrograph RH Veloce 200, manufactured by Officina Stellare, Italy. This unique optics has a focal length of 600 mm and an aperture of 216 mm, providing a focal ratio of $f/3$. In addition, the image acquisition is done by a CCD camera of FLI MicroLine KAF 8300 camera with an array of 3326x2504 pixels of 5.4 microns providing an angular resolution of 1.86 arcsec/pixel and a field of

view of approximately 1.2×1.6 degrees. The global mechanical shutter is remotely triggered with a TTL signal generated by a ublox GNSS receiver.

The tiltmeter part is formed by two pairs of precise tiltmeters mounted orthogonally. The tilting part describing the relation between the optical rotation axis and the local plumb line consists of two pairs of tiltmeters. The first pair is of type Zerotronic manufactured by Wyler AG Winterthur, Switzerland. The second sensor pair consists of two High Resolution Tilt Meters (HRTM), manufactured by Erich Lippmann, Schaufling, Germany. During the acquisition, the data are continuously recorded at a rate of 10 Hz.

The mechanical automation is done by 4 motors which control the extension of the electromechanical legs for the initial setup, the precise automatic levelling and the rotation of the superstructure into two faces.

The data acquisition on a station starts with an automatic levelling of the system at a level better than 5 arcsecond. Then, after checking the connections to the sensors and the focusing the data collection begins. The superstructure is rotated by 180 degrees around its vertical axis in order to eliminate most of the radial symmetric errors. In opposition to the DIADEM system, this setup is repeated 4 times. Each time the complete system is rotated by 90 degrees. This strategy permits to eliminate residual systematic effects due to the mechanical angular variations which can appear when the superstructure is rotated. At the end of a station observation, approximately 150 sky-images are stored on the computer. Approximately 8000 stars are identified for each station (Fig. 13) and processed with the corresponding filtered tiltmeter.

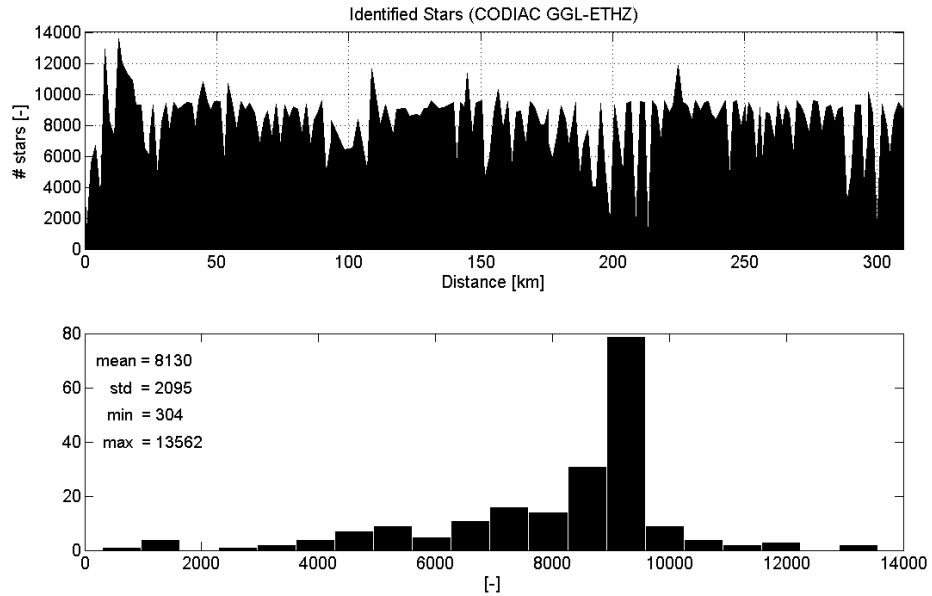


Fig. 13 Number of stars which are identified per single station for the campaign GSVS14.

The computation of the DoV are performed in the software AURIGA (Hirt 2004) whereas the tilt values are previously filtered, predicted, rectified with the calibration parameters (determined every day with a celestial calibration procedure) and combined in a least-squares collocation strategy. Prior to the final combination, the values from the Wyler and the Lippmann sensors can be compared. This comparison provides an independent check on tilt corrections (Fig. 14).

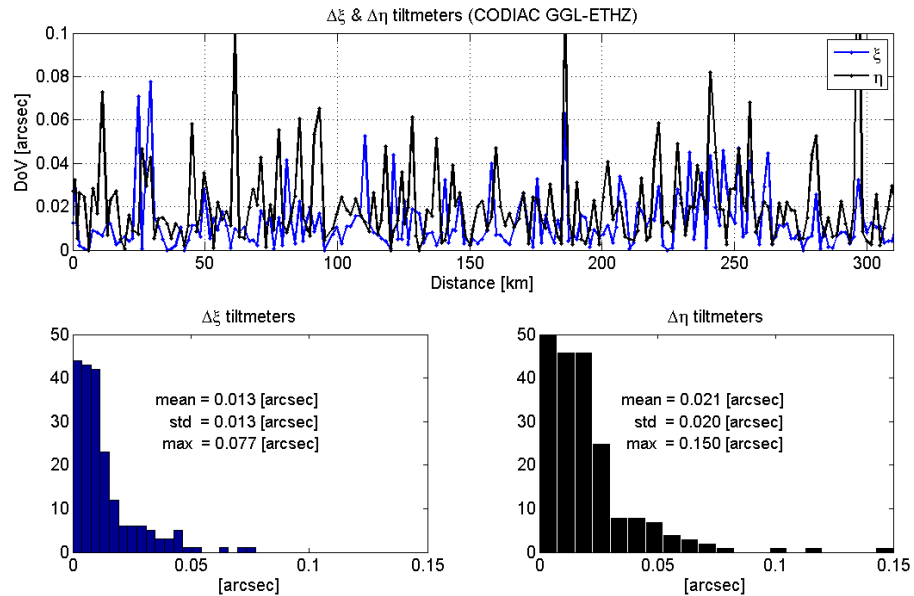


Fig. 14 Mean differences between the tiltmeters corrections provided by the Wyler and the Lippmann systems for the campaign GSVS14.

Acknowledgements. The following NGS staff participated in the survey and sincerely acknowledged: Roy Anderson, James Richardson, Kendall Fancher, Don Breidenbach, T Hanson, Brian Shaw, Robert Hayes, Doug Adams, Courtney Lindo, Jim Tomlin, Simon Monroe, Eric Duvall, Tim Wilkins, Dan Callahan, Jim Harrington, Kevin Jordan, David Grosh, Phillip Marshall, Clyde Dean, Justin Dahlberg, Chris Villareal, Mark Schenewerk, Carly Weil, Simon Holmes, and Rick Foote. Discussions with Dr. Dru Smith and Mr. Jarir Saleh are important to improve the quality of the paper.

References

Bossler J (1984) FGCC Standards and Specifications for Geodetic Control Networks, Library of Congress

Flury J (2016) Relativistic geodesy, 8th Symposium on Frequency Standards and Metrology 2015
 Fritz Riehle 2016 Journal of Physics: Conference Series **723** 011001

Forsberg R (1984) A study of terrain reductions, density anomalies and geophysical inversion methods in gravity field modelling. Reports of the Department of Geodetic Science and Surveying, #355. The Ohio State University, Columbus, Ohio

Guillaume S (2015) Determination of a Precise Gravity Field for the CLIC Feasibility Studies. Ph.D. Thesis, Eidgenössische Technische Hochschule ETH Zürich, Nr. 22590. <http://dx.doi.org/10.3929/ethz-a-010549038>

Heiskanen WA and Moritz H (1967) Physical geodesy. Freeman, San Francisco

- Higgins MB, MB Pearse and AHW Kearsley (1996) Using digital elevation models in the computation of geoid heights. *Geomatics Research Australasia* (1996): 59-74.
- Hirt C (2004), Entwicklung und Erprobung eines digitalen Zenitkamarasystems für die hochpräzise Lotabweichungsbestimmung, Ph.D. thesis, Universität Hannover.
- Hirt C and Flury J (2008) Astronomical-topographic levelling using high-precision astrogeodetic vertical deflections and digital terrain model data, *J Geod* 82:231–248
- Hoffmann-Wellenhof B and H Moritz (2006) *Physical Geodesy*. Springer, Wien New York
- Li X, JW Crowley, SA Holmes, and YM Wang (2016) The contribution of the GRAV-D airborne gravity to geoid determination in the Great Lakes region, *Geophys. Res. Lett.*, 43, 4358–4365
- Jekeli (1999) An analysis of vertical deflections derived from high-degree spherical harmonic models, *J Geoid*. 73:10-22
- Jiang T and YM Wang (2016) On the spectral combination of satellite gravity model, terrestrial and airborne gravity data for local gravimetric geoid computation, *J Geod*, in printing
- Moritz H (1980) *Advanced physical geodesy*. Herbert Wichmann Verlag, Karlsruhe
- Mayer-Gürr T. et al. (2012) The new combined satellite only model GOCO03s. SSS2012, Venice
- Mayer-Gürr T. et al. (2015) The combined satellite gravity field model GOCO05s. Presentation at EGU 2015, Vienna, April 2015
- Pavlis NK, SA Holmes, SC Kenyon, and JK Factor (2012) The development and evaluation of the Earth Gravitational Model 2008 (EGM2008), *J. Geophys. Res.*, 117, B04406, doi:10.1029/2011JB008916
- Smith DA , Holmes SA, Li XP, Guillaume S, Wang YM, Bürki B, Roman DR, Damiani TM (2013) Confirming regional 1 cm differential geoid accuracy from airborne gravimetry: the Geoid Slope Validation Survey of 2011. *J Geod* 87: 885-907
- Somieski, AE (2008), Astrogeodetic geoid and isostatic considerations in the north aegean sea, greece, Ph.D. Thesis, , Eidgenössische Technische Hochschule ETH Zürich, Nr. 17790.
- Wang YM, D Martin and G Mader (2016) Search Results for: NGS Finds Real Time Solution in Iowa – Iowa RTN Contributes to Geoid Slope Validation Survey of 2014, *xyHt* January 2016 Issue p. 24-27

Wang YM, X Li, S Holmes, DR Roman, DA Smith (2013) Investigation of the use of deflections of vertical measured by DIADEM camera in the GSVS11 Survey, EGU General Assembly 2013, held 7-12 April, 2013 in Vienna, Austria, id. EGU2013-12779

Zilkoski DB, JH Richards, and GM Young (1988) Results of the General Adjustment of the North American Vertical Datum of 1988. *Surv Land Inf Syst* 52(3):133-149